IMMUNOLOGY

Gasdermin D in macrophages restrains colitis by controlling cGAS-mediated inflammation

Chunmei Ma[1]*, Dongxue Yang[1]*, Bingwei Wang[2]*†, Chunyan Wu[1], Yuqing Wu[1], Sheng Li[1], Xue Liu[1], Kara Lassen[3], Lue Dai[4]†, Shuo Yang[1]†

The functional relevance and mechanistic basis of the effects of the pyroptosis executioner Gasdermin D (GSDMD) on colitis remain unclear. In this study, we observed that GSDMD protein was activated during intestinal inflammation in a model of chemically induced colitis. GSDMD deficiency exacerbated experimental colitis independent of changes in the microbiota and without affecting the production of antimicrobial peptides. GSDMD deficiency in macrophages, but not epithelial cells, was sufficient to drive this exacerbated experimental colitis. We further demonstrate that GSDMD functions in macrophages as a negative regulator to control cyclic GMP–AMP synthase (cGAS)–dependent inflammation, thereby protecting against colitis. Moreover, the administration of cGAS inhibitor can rescue the colitogenic phenotype in GSDMD-deficient mice. Collectively, these findings provide the first demonstration of GSDMD's role in controlling colitis and a detailed delineation of the underlying mechanism.

INTRODUCTION

Inflammatory bowel diseases (IBDs), including Crohn's disease (CD) and ulcerative colitis, are chronic and complex disorders characterized by uncontrolled intestinal pathogenic inflammation and intestinal tissue injury (*1*). Incidences of IBD are increasing around world, and current therapies maintain remission in a subset of individuals but cannot completely control inflammation and IBD relapse (*2*). Normally, the gut mucosal immune system coevolves with the intestinal bacteria, acquiring the capacity to tolerate the components of bacteria and maintaining the capacity to respond to invading pathogens (*3*). In addition, most intestinal bacteria are considered commensal to the host for contributing to the development and homeostasis of intestinal immune system (*4*). The intestinal mucosal immune system, which is mainly composed of the intestinal epithelium and lamina propria (LP), mediates the production of mucin and bactericidal molecules and induces immune response, thereby providing the effective defense line against invading bacteria (*5*). Dysfunction of the intestinal mucosal system exposes immune cells to excessive bacteria load, leading to an inflammatory state associated with violent responses to microbe-associated molecular patterns and a subsequent large amount of proinflammatory cytokines (*6*).

The intestinal mucosal immune system uses several innate receptors, including Toll-like receptors, nucleotide-binding oligomerization domain protein-like receptors (NLRs), and C-type lectin receptors, to monitor bacterial colonization and regulate mucosal immune homeostasis (*7*). Among these receptors, NLR proteins, such as NLRP1, NLRP3, NLRC4, and NLRP6, are assembled into cytosolic multiprotein complexes termed as inflammasomes together with apoptosis-associated speck-like protein (ASC) and proinflammatory caspases (caspase-1 and caspase-11), which leads to caspase autoactivation that governs the cleavage of pro–interleukin-1β (IL-1β) and pro–IL-18 precursors into their mature forms and also induces a type of proinflammatory programmed cell death termed as pyroptosis (*8*, *9*). The IL-1 family of cytokines has been reported to regulate intestinal homeostasis, inflammation, and healthy microbiota (*10*, *11*). Specifically, NLRP3 inflammasome induces IL-1β in myeloid cells, which promotes intestinal inflammation with the accumulation of innate lymphoid cells (ILCs) and T helper 17 (T_H17) cells (*12*, *13*), whereas IL-18, processed by NLRP6 inflammasome, protects intestinal epithelial cells (IECs) against colitis with enhanced intestinal epithelial integrity and secretion of antimicrobial peptides (AMPs) (*14*). Nevertheless, a recent study showed that IL-18 contributes to a pathologic breakdown of the intestinal barrier by inhibiting goblet cell maturation (*15*). In general, the inflammasome-related proteins, especially NLRP6, ASC, or caspase-1, are thought to play protective roles in experimental colitis in a microbiota-dependent manner (*16*). Consistent with this hypothesis, NLRP6 has been reported, together with ASC and caspase-1 or caspase-11, to regulate mucin granule exocytosis and maintain the mucosal integrity through autophagy in goblet cells (*17*). However, recent research has suggested that the NLRP6 inflammasome may not be required for the formation or function of baseline colonic inner mucus layer (*18*). As such, the functions of inflammasome in mucosal immunity and colitis seem complicated, and their underlying mechanisms remain not well understood.

Gasdermin D (GSDMD) is a newly identified pyroptosis executioner that operates downstream of inflammasome activation (*19*). Upon activation, proinflammatory caspases (caspase-1 and caspase-4/5 in humans and caspase-1 and caspase-11 in mice) cleave GSDMD in its central linker domain. Once cleaved, the N-terminal domain of GSDMD (GSDMD-N) is released from the autoinhibition by the C-terminal domain of GSDMD (GSDMD-C). Next, GSDMD-N fragments oligomerize and translocate to the plasma membrane and form pores, which induces cell lytic death and the secretion of IL-1β and IL-18 (*20*). GSDMD has been linked to potential pathogenesis of some diseases such as septic shock and experimental autoimmune encephalomyelitis (EAE) (*21*, *22*). A more recent study has revealed how GSDMD restrains cGAS-dependent inflammation (*23*). Moreover, GSDMD mediates IEC pyroptosis, which may be required for removing pathogen-infected epithelial cells (*24*). However, the exact function of

[1]Department of Immunology, Key Laboratory of Immunological Environment and Disease, State Key Laboratory of Reproductive Medicine, Center for Global Health, Nanjing Medical University, Nanjing, China. [2]Department of Pharmacology, Nanjing University of Chinese Medicine, Nanjing, China. [3]Roche Innovation Center Basel, Basel, Switzerland. [4]Roche Innovation Center Shanghai, Shanghai, China.
*These authors contributed equally to this work.
†Corresponding author. Email: shuoyang@njmu.edu.cn (S.Y.); lue.dai@roche.com (L.D.); bingweiwang@njucm.edu.cn (B.W.)

GSDMD in the context of colitis is largely unknown. In this study, we sought to understand the role of GSDMD in colitis and elucidate underlying mechanisms.

RESULTS

GSDMD is highly activated in the intestine of dextran sodium sulfate–treated mice

GSDMD protein was found highly expressed in various tissues of mice, especially mesenteric lymph nodes (mLNs) and intestine (Fig. 1A). Immunofluorescence analysis showed wide distribution of GSDMD in both LP Cx3cr1$^+$ myeloid cells (tdTomato reporter) and epithelial E-cadherin$^+$ cells (Fig. 1B). To further investigate whether GSDMD has a possible role in intestinal inflammation, we used the dextran sodium sulfate (DSS) model of colitis. Briefly, mice were given 2.5% DSS in the drinking water for 6 days and then switched to normal drinking water until day 9. We tested GSDMD and caspase-11 expression on day 9 in both control and DSS-treated mice. Immunoblotting analysis revealed the substantially increased expression and cleavage of GSDMD and caspase-11 in the colon of colitis mice relative to untreated mice (Fig. 1C). We next isolated IECs and myeloid cells from colons of colitis mice to investigate GSDMD activation in these cells. We found that the more notable GSDMD activation induced by colitis in myeloid cells was mainly characterized by a 30-kDa cleaved fragment, whereas both p30 and p47 fragments are the major cleaved bands in IECs (Fig. 1D). Collectively, these results suggest the involvement of GSDMD-mediated pyroptosis in this colitis model.

GSDMD deficiency exacerbates DSS-induced colitis

To directly evaluate the role of GSDMD in colitis, we treated age-matched GSDMD knockout (*GSDMD*$^{-/-}$) or wild-type (WT) mice with DSS to compare their colitis phenotype. The *GSDMD*$^{-/-}$ mice exhibited normal growth and survival, and GSDMD deficiency did not affect the development and maturation of myeloid and lymphoid cells in central and peripheral lymphoid organs under homeostatic conditions, as previously reported by our laboratory (*21*). Notably, a more severe colitis on day 9 after DSS administration was observed in *GSDMD*$^{-/-}$ mice than in WT controls, as characterized by significantly greater body weight loss, higher disease activity index (DAI) score, and shorter colons in DSS-treated *GSDMD*$^{-/-}$ mice (Fig. 1, E to G). Consistently, histopathological analysis [hematoxylin and eosin (H&E) staining] showed that GSDMD deficiency led to increased inflammatory cell infiltration with a more severe disruption of the mucosal epithelium in response to DSS treatment (Fig. 1H). In addition, we used ASC knockout (*ASC*$^{-/-}$) mice as a control and confirmed the protective effect of inflammasome on colitis, as previously reported (Fig. 1, I to L) (*16*). Together, these data suggest that similar to other inflammasome proteins, GSDMD plays a protective role in DSS-induced colitis.

GSDMD deficiency drives severe DSS colitis in a microbiota-independent manner

Loss of inflammasome components, such as NLRP6 and ASC, led to the shift of microbial communities toward a transmissible and more colitogenic microbiota that drives DSS-induced colitis (*16*). To evaluate whether the increased severity in colitis observed in *GSDMD*$^{-/-}$ mice relative to WTs is also driven by colitogenic microbiota, we cohoused littermate WT mice [WT (*GSDMD*$^{-/-}$)] and *GSDMD*$^{-/-}$ mice [*GSDMD*$^{-/-}$ (WT)] for 6 weeks to equalize bacterial community before administration of DSS. Analysis of bacterial 16*S* ribosomal RNA (rRNA) sequencing of fecal pellets demonstrates similar bacterial composition including comparable bacterial diversity and abundance in family levels (including the colitogenic Prevotellaceae and Bacteroidales) between the cohoused WT and *GSDMD*$^{-/-}$ mice (fig. S1, A to C). Cohousing breeding did not change the development of more severe DSS-induced colitis in *GSDMD*$^{-/-}$ (WT) mice as compared with the cohoused WT (*GSDMD*$^{-/-}$) controls (fig. S2, A to D). While cohousing of littermate WT mice [WT (*ASC*$^{-/-}$)] and *ASC*$^{-/-}$ [*ASC*$^{-/-}$(WT)] also led to similar bacterial diversity and abundance (fig. S1, D to F), this now almost equalized the severity of DSS-induced colitis (fig. S2, E to H). Therefore, unlike ASC, GSDMD protects against colitis independent of gut microbiota changes.

GSDMD deficiency exacerbates colonic inflammation but does not impair the production of AMPs and mucus secretion

To further characterize the role of GSDMD in colitis as a negative regulator of intestinal inflammation, we analyzed the expression of proinflammatory cytokines and chemokines in colon explants of WT and *GSDMD*$^{-/-}$ colitis mice by real-time quantitative polymerase chain reaction (RT-qPCR) and enzyme-linked immunosorbent assay (ELISA). GSDMD deficiency significantly increased the production of proinflammatory cytokines and chemokine including IL-6, tumor necrosis factor–α (TNF-α), interferon-β, and Ccl2, and as expected, the secretion of IL-1β and IL-18 was impaired in the absence of GSDMD (Fig. 2, A and B, and fig. S3, A and B). Moreover, fluorescence-activated cell sorting (FACS) revealed a significant increase in the frequencies and absolute numbers of colon-infiltrating immune cells (CD45$^+$), CD4$^+$ and CD8$^+$ T cells, macrophages (CD11b$^+$F4/80$^+$), monocytes (CD11b$^+$Ly6c$^+$), and neutrophils (CD11b$^+$Ly6g$^+$) in *GSDMD*$^{-/-}$ mice relative to those in WT mice on day 5 after DSS treatment (Fig. 2, C and D). Moreover, we observed a reduction in PI$^+$ cells gated on the CD45$^+$CD11b$^+$F4/80$^+$ (colonic macrophages) in the colon of *GSDMD*$^{-/-}$ mice during colitis compared with control mice (Fig. 2E). Thus, GSDMD deficiency promotes colonic inflammation and protects colonic macrophages from death during colitis.

Inflammasome is expected to shape the composition of microbiome to avoid the outgrowth of colitogenic bacteria by regulating the production of AMPs (*14*). Next, we investigated whether GSDMD affects the expression of AMPs and its inducing cytokine IL-22 but found no significant difference in the expression of *Il22* or AMPs, such as *Reg3b*, *Reg3g*, *Defn5*, and *Lysozyme1*, between the colons of untreated (fig. S3C) and DSS-treated (Fig. 2F) WT and *GSDMD*$^{-/-}$ mice. Because intestinal mucosal barrier integrity is also important in host defense against colitis (*25*) and NLRP6 inflammasome and IL-18 can regulate mucin granule exocytosis and goblet cell maturation to affect intestinal barrier function (*15*, *17*), we further assessed whether GSDMD affects the expression or secretion of mucus proteins in goblet cells. We found no difference in the expression of mature goblet cell mucin MUC2 in colons from WT and *GSDMD*$^{-/-}$ mice untreated (fig. S3C) or treated with DSS (Fig. 2F). Moreover, Periodic acid–Schiff (PAS) and MUC2 staining showed the comparable abundance and configuration of mature PAS$^+$ and MUC2$^+$ goblet cells in untreated (fig. S3, D and E) or DSS-treated (Fig. 2, G and H) WT and *GSDMD*$^{-/-}$ mice. Together, these data suggest that GSDMD has no impact on the production of AMPs and mucus but is indispensable in controlling colonic inflammation.

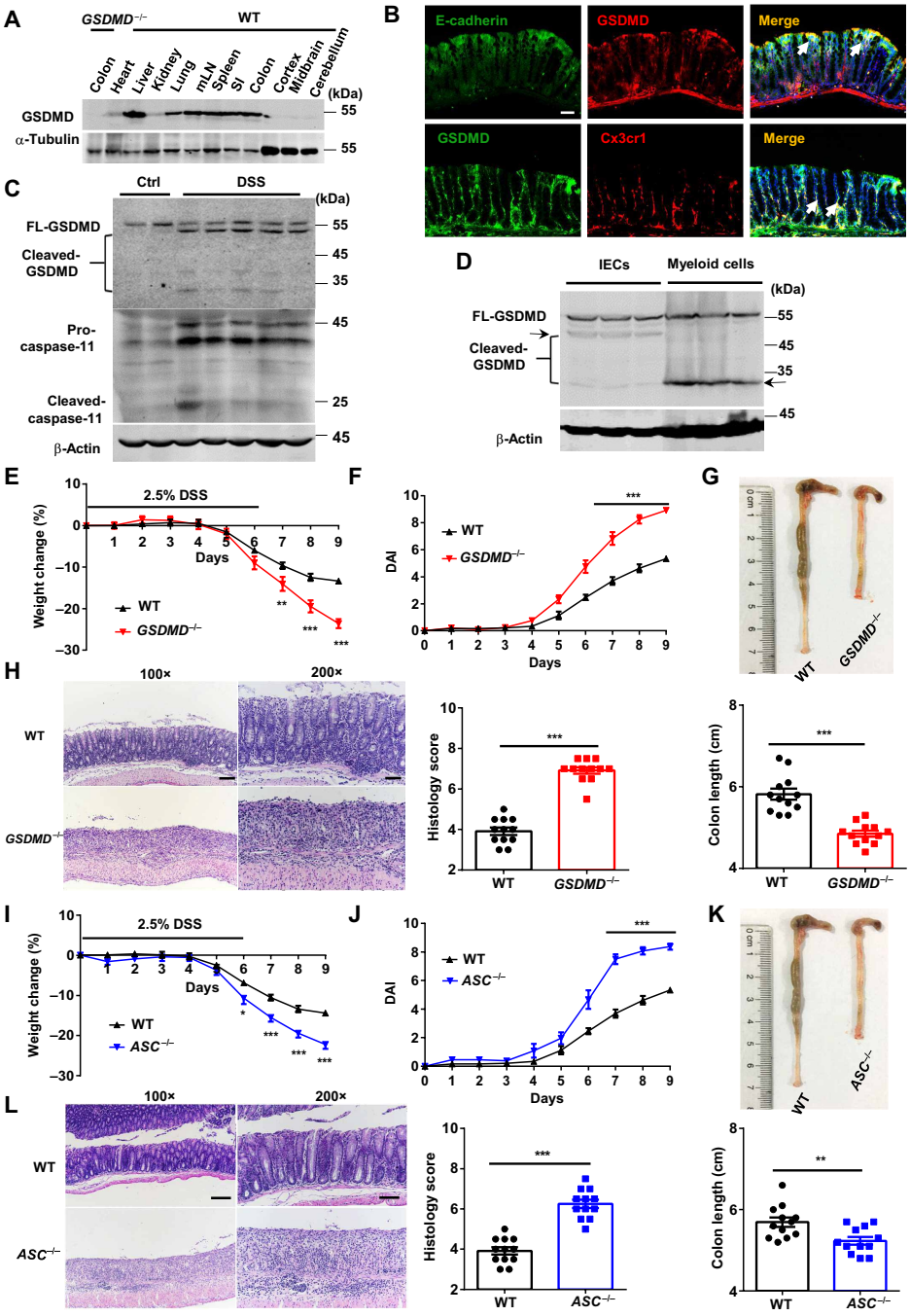

Fig. 1. GSDMD is activated in the intestine of DSS-induced colitis mice and protects against DSS-induced colitis. (**A**) Immunoblot analysis of GSDMD expression in various organs, including heart, liver, kidney, lung, mLNs, spleen, small intestine (SI), colon, cortex, midbrain, and cerebellum from *GSDMD*$^{-/-}$ and wild-type (WT) mice. (**B**) Immunofluorescence labeling of GSDMD (red), 4′,6-diamidino-2-phenylindole (DAPI) (blue) in colon sections from WT mice, and labeling of GSDMD (green), Cx3cr1 (red), and DAPI (blue) in colon sections from Cx3cr1 reporter mice. The merging of GSDMD with E-cadherin or Cx3cr1 is indicated by arrows. Scale bar, 200 μm. (**C**) Immunoblot analysis of full-length and cleaved GSDMD and caspase-11 in colon from control or DSS-treated WT mice on day 9. (**D**) Immunoblot analysis of full-length and cleaved GSDMD in IECs and myeloid cells sorted from colon of DSS-treated WT mice on day 9. (**E** and **F**) Age-matched male WT ($n = 12$) and *GSDMD*$^{-/-}$ ($n = 12$) mice were given 2.5% DSS in their drinking water for 6 days and then normal water for three further days. Weight changes (E) and DAI (F) were monitored daily. (**G**) Gross morphology images of colons and colon lengths of WT and *GSDMD*$^{-/-}$ mice on day 9 after DSS treatment. (**H**) Representative H&E staining of distal colon sections and histology scores of WT and *GSDMD*$^{-/-}$ mice on day 9 after DSS treatment. Scale bars, 100×, 100 μm; 200×, 200 μm. (**I** and **J**) Daily weight changes (H) and DAI (I) of WT ($n = 12$) and *ASC*$^{-/-}$ ($n = 12$) mice treated with 2.5% DSS. (**K**) Gross morphology images of colons and colon lengths of WT and *ASC*$^{-/-}$ mice on day 9 after DSS treatment. (**L**) Representative H&E staining of distal colon sections and histology scores of WT and *ASC*$^{-/-}$ mice sampled on day 9 after DSS treatment. Scale bars, 100×, 100 μm; 200×, 200 μm. Data are representative of three independent experiments (A and B). Data are pooled from three independent experiments for (E) to (L). Error bars show means ± SEM. *$P < 0.05$, **$P < 0.01$, and ***$P < 0.001$. Two-way analysis of variance (ANOVA) with Sidak's multiple comparisons test for weight changes and DAI and two-tailed unpaired Student's *t* test for colon length and histology scores. Photo credit: (G) and (K) were taken by D.Y. (Department of Immunology, Nanjing Medical University).

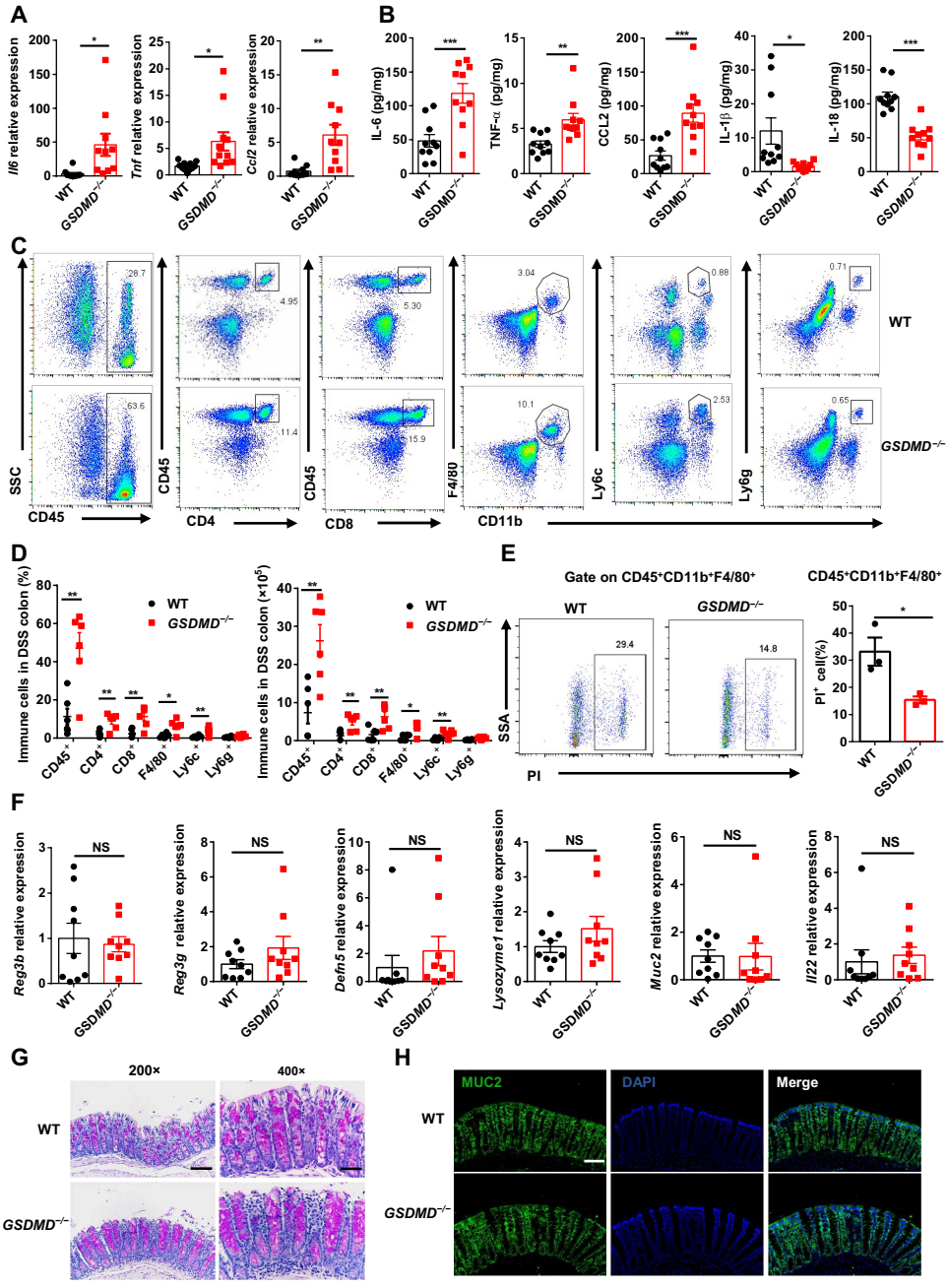

Fig. 2. GSDMD deficiency exacerbates colonic inflammation but does not impair the production of AMPs and mucus secretion. (**A**) RT-qPCR analysis of the relative mRNA expression of *Il6*, *Tnf*, and *Ccl2* mRNA levels in colonic tissues of WT and *GSDMD*$^{-/-}$ mice ($n = 10$ mice per group) on day 9 after DSS treatment. (**B**) ELISA of IL-6, TNF-α, CCL2, IL-1β, and IL-18 protein levels in supernatant of colonic explants of WT and *GSDMD*$^{-/-}$ mice ($n = 10$ mice per group) on day 9 after DSS treatment. (**C** and **D**) Flow cytometric analysis of colon-infiltrated immune cells of WT and *GSDMD*$^{-/-}$ mice ($n = 6$ mice per group) on day 5 after DSS treatment. Data are presented as representative plots (C) and summary graphs of quantified percentages and absolute cell numbers (D). SSC, side scatter. (**E**) Flow cytometric analysis of PI^{+} cells gated on the CD45^{+}CD11b^{+} F4/80^{+} in colons of WT and *GSDMD*$^{-/-}$ mice on day 5 after DSS treatment ($n = 3$ mice per group). Data are presented as a representative plot (left) and quantified percentages (right). (**F**) RT-qPCR analysis of the relative mRNA expression of AMPs (*Reg3b*, *Reg3g*, *Defn5*, *Lysozyme1*, and *Muc2*) and *Il22* in colons of WT ($n = 9$) and *GSDMD*$^{-/-}$ ($n = 9$) mice on day 9 after DSS treatment. (**G**) PAS staining of distal colon sections of WT and *GSDMD*$^{-/-}$ mice on day 5 after DSS treatment. Scale bars, 200×, 200 μm; 400×, 400 μm. (**H**) Immunofluorescence labeling of MUC2 (green) and DAPI (blue) in WT and *GSDMD*$^{-/-}$ mice on day 5 after DSS treatment. Scale bar, 200 μm. Data are pooled from three independent experiments (A to D and F to H) or from two independent experiments (E). Error bars show means ± SEM. *$P < 0.05$, **$P < 0.01$, and ***$P < 0.001$; NS, not significant. Two-tailed unpaired Student's *t* test.

GSDMD in macrophages controls DSS-induced colitis

To determine whether GSDMD deficiency in IECs or hematopoietic cells contributes to the more severe colitis phenotype, we measured the expression of GSDMD in the isolated epithelial and LP hematopoietic cells from colon and found that GSDMD was expressed in both, but higher expression was observed in epithelial cells (fig. S4, A and B). Thus, we first examined whether the protective role of GSDMD in colitis was intrinsic to IECs by crossing the *GSDMD*$^{fl/fl}$ mice with *Villin*-Cre mice to generate epithelium conditional knockout mice of GSDMD (*GSDMD*$^{fl/fl}$*Villin*-Cre). *GSDMD*$^{fl/fl}$*Villin*-Cre and littermate control *GSDMD*$^{fl/fl}$ mice demonstrated similar weight loss, DAI, colon shortening, and histopathology after DSS treatment (Fig. 3, A to D and fig. S4C), and therefore, GSDMD in epithelium seems not a protective factor in the pathogenesis of DSS-induced colitis. Given the known functions of GSDMD in myeloid cells and the pivotal roles of innate immune cells in the development of colitis (*26*, *27*), we then generated myeloid cell conditional knockout mice of GSDMD by crossing the *GSDMD*$^{fl/fl}$ mice with *LysM*-Cre mice (*GSDMD*$^{fl/fl}$*LysM*-Cre). We observed greater body weight loss and higher DAI score in *GSDMD*$^{fl/fl}$*LysM*-Cre mice relative to littermate control *GSDMD*$^{fl/fl}$ mice after DSS treatment (Fig. 3, E and F, and fig. S4D). The colon length of *GSDMD*$^{fl/fl}$*LysM*-Cre mice was much shorter than that of *GSDMD*$^{fl/fl}$ mice (Fig. 3G). Moreover, increased infiltrating inflammatory cells and a more severe disruption of the mucosal epithelium in response to DSS treatment were observed in *GSDMD*$^{fl/fl}$*LysM*-Cre mice, as shown by H&E staining (Fig. 3H). In addition, the expression of inflammatory cytokines and chemokines was markedly increased in colon of *GSDMD*$^{fl/fl}$*LysM*-Cre mice (fig. S5A and B). Collectively, these results support the notion that GSDMD in myeloid cells is essential for its protective role in DSS-induced colitis.

Because *LysM*-Cre–mediated recombination results in the deletion of a targeted gene in the myeloid cell lineage, including macrophages and neutrophils (*28*), we intravenously injected anti-Ly6G antibody (α-Ly6G) into *GSDMD*$^{fl/fl}$*LysM*-Cre and littermate control *GSDMD*$^{fl/fl}$ mice to deplete neutrophils before DSS treatment. In the absence of neutrophils, GSDMD deficiency still exacerbated the colitis phenotype as indicated by increased body weight loss, higher DAI score, shorter colon length, and colon-infiltrating immune cells (Fig. 3, I to M), suggesting that the function of GSDMD in macrophages negatively regulates the colitis phenotypes.

GSDMD deficiency enhances the cGAS-dependent inflammation in colonic macrophages during colitis

To further dissect the mechanistic role of GSDMD in macrophages that protect against colitis, we performed RNA sequencing (RNA-seq) analysis using CD11b$^+$F4/80$^+$ cells sorted from colon LP of WT and *GSDMD*$^{-/-}$ mice at onset stage of DSS-induced colitis (Fig. 4A). The Kyoto Encyclopedia of Genes and Genomes (KEGG) analysis showed that one of the top pathways up-regulated in *GSDMD*$^{-/-}$ CD11b$^+$F4/80$^+$ cells was cytosolic DNA-sensing pathway, in which cytosolic DNA is sensed by cGAS and triggers inflammatory response (Fig. 4B). Gene Set Enrichment Analysis (GSEA) and Gene Network Analysis further highlight the critical role of GSDMD in the regulation of genes involved in the DNA-sensing pathway (Fig. 4, C and D). Consistent with this, the heatmap and RT-PCR analysis displayed significantly increased expression in many genes associated with cGAS-dependent inflammation, such as *Ifit1*, *Oasl2*, *Irf7*, *Irf3*, *Ddx41*, *Il6*, *Tnf*, *Ccl20*, *Ccl4*, and *Ccl5*, in *GSDMD*$^{-/-}$ cells (Fig. 4, E and F). We next measured the concentrations of cGAMP in WT and *GSDMD*$^{-/-}$ colonic tissues during colitis and detected higher levels of cGAMP in *GSDMD*$^{-/-}$ colonic tissues than that in WTs (Fig. 4G). Moreover, we observed the greatly increased phosphorylation of STING, TBK1, and IRF3 in the *GSDMD*$^{-/-}$ colonic tissues compared with controls after DSS challenge (Fig. 4H). As previously reported (*29*), the cGAS-STING signaling can trigger the activation of transcription factors IRF3 and nuclear factor κB, thereby enhancing the transcription of targeted genes encoding interferons, and proinflammatory cytokines and chemokines, respectively. Together, these data suggest a model whereby GSDMD restricts cGAS-mediated inflammatory response in macrophages during early colitis. Notably, GSDMD in macrophages can restrain cGAS-dependent inflammation in response to cytosolic DNA or *Francisella novicida* bacterial infection (*23*). To investigate whether GSDMD in colonic macrophages negatively regulates such cGAS-dependent inflammation, we treated CD11b$^+$F4/80$^+$ cells isolated from colon of WT and *GSDMD*$^{-/-}$ mice with cGAS activator, including genomic DNA (gDNA) or poly(deoxyadenylic-deoxythymidylic) [poly(dA:dT)]. Accordingly, we detected higher levels of IL-6, TNF-α, Ccl2, and Ccl5 production in response to gDNA or poly(dA:dT) in colonic macrophages from *GSDMD*$^{-/-}$ mice than those from WT mice (Fig. 5, A and B, and fig. S6, A and B). Moreover, treatment with a cGAS inhibitor RU.521 (*30*) could significantly inhibit the elevated production of IL-6, TNF-α, and Ccl5 in *GSDMD*$^{-/-}$ cells (Fig. 5, C and D). Collectively, these data suggest a negative role of GSDMD in colonic macrophages in regulating cGAS-dependent inflammation.

The administration of cGAS inhibitor restricts colitis in *GSDMD*$^{-/-}$ mice

Because cGAS-STING signaling has been shown to promote intestinal inflammation (*31*), we speculated that GSDMD may restrict colitis by restraining cGAS-mediated inflammation. To test this hypothesis, we treated WT and *GSDMD*$^{-/-}$ mice with intraperitoneal administration of the cGAS inhibitor RU.521. Such treatment significantly attenuated the clinical signs of colitis in WT mice as indicated by less weight loss, lower DAI score, less shortening in colon length, and less histopathological findings (Fig. 6, A to E). More notably, it completely rescued colitis phenotype in *GSDMD*$^{-/-}$ mice to comparable levels in RU.521-treated WT mice (Fig. 6, A to E). Moreover, the treatment of cGAS inhibitor RU.521 can significantly reduce cGAMP and the phosphorylation of STING, TBK1, and IRF3 in the *GSDMD*$^{-/-}$ colonic tissues to comparable levels in RU.521-treated WTs during colitis (Fig. 6, F and G). Thus, all these data suggest that the protective role of GSDMD in colitis is dependent on its controlling cGAS-mediated inflammation.

DISCUSSION

In this study, we comprehensively dissect the role of GSDMD protein, a key pyroptosis executioner, in the context of experimental colitis. We found that GSDMD protein was activated in the colon of colitis mice, and that GSDMD in macrophages confers protection against experimental colitis through restricting cGAS-dependent inflammation.

Over the years, many studies have tried to understand the roles of inflammasome in colitis. A variety of studies showed that, with the exception of NLRP3, most inflammasome-related proteins,

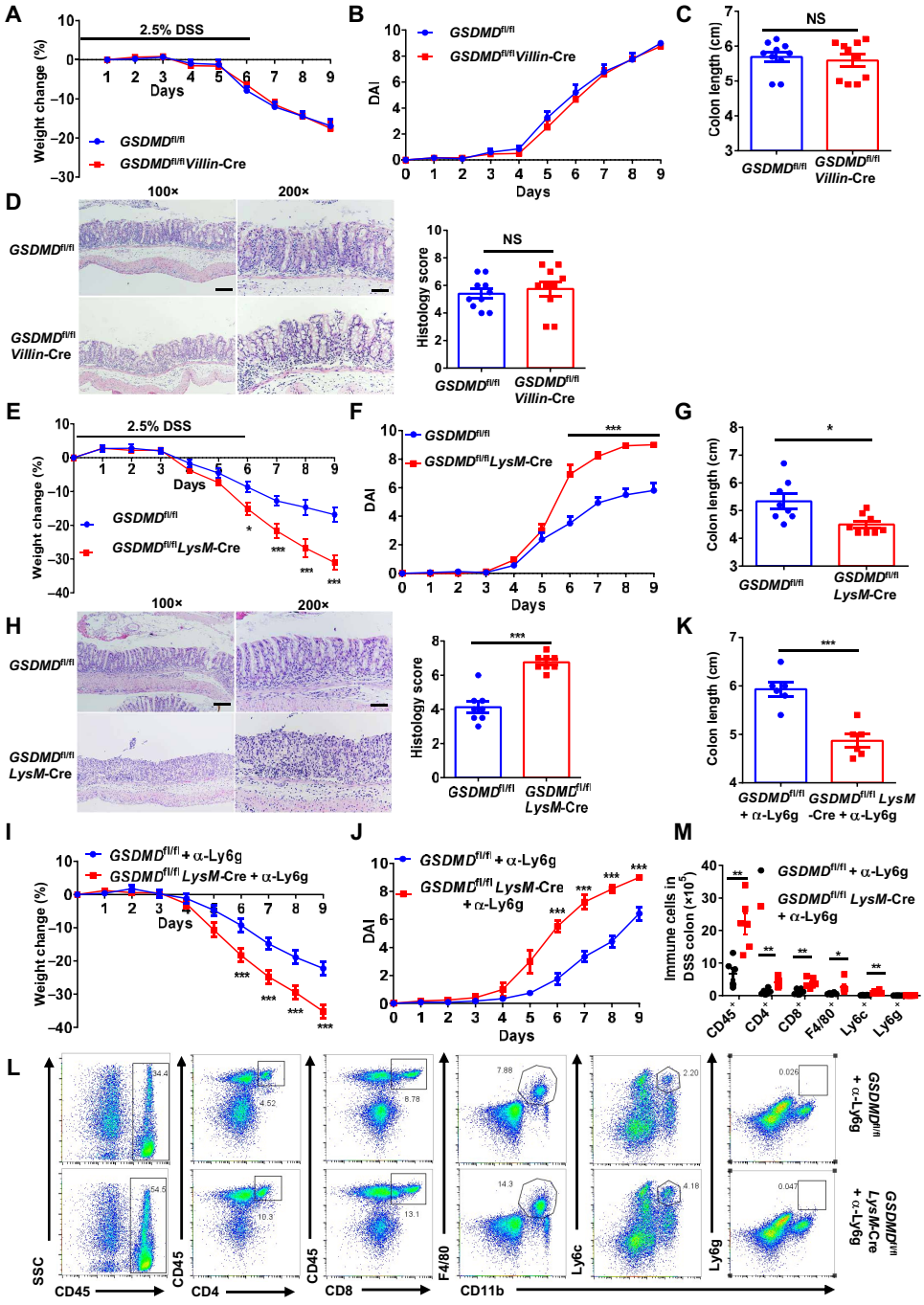

Fig. 3. Macrophage-intrinsic GSDMD controls DSS-induced colitis. (**A** and **B**) Weight changes (A) and DAI (B) of *GSDMD*$^{fl/fl}$*Villin*-Cre and littermate control *GSDMD*$^{fl/fl}$ mice ($n = 10$ mice per group) after colitis induction. (**C**) Colon lengths of *GSDMD*$^{fl/fl}$*Villin*-Cre and littermate control *GSDMD*$^{fl/fl}$ mice on day 9 after DSS treatment. (**D**) Representative H&E staining of distal colon sections and histology scores of *GSDMD*$^{fl/fl}$*Villin*-Cre and littermate control *GSDMD*$^{fl/fl}$ mice sampled on day 9 after DSS treatment. Scale bars, 100×, 100 μm; 200×, 200 μm. (**E** and **F**) Weight changes (E) and DAI (F) of *GSDMD*$^{fl/fl}$*LysM*-Cre and littermate control *GSDMD*$^{fl/fl}$ mice ($n = 8$ mice per group) after colitis induction. (**G**) Colon lengths of *GSDMD*$^{fl/fl}$*LysM*-Cre and *GSDMD*$^{fl/fl}$ mice on day 9 after DSS treatment. (**H**) Representative H&E staining of distal colon sections and histology scores of *GSDMD*$^{fl/fl}$*LysM*-Cre and *GSDMD*$^{fl/fl}$ mice on day 9 after DSS treatment. Scale bars, 100×, 100 μm; 200×, 200 μm. (**I** to **K**) *GSDMD*$^{fl/fl}$*LysM*-Cre and littermate control *GSDMD*$^{fl/fl}$ mice ($n = 6$ mice per group) were intravenously injected with anti-Ly6g antibody to delete CD11b^{+}Ly6g^{+} neutrophils during DSS treatment. Weight changes (I), DAI (J), and colon lengths (K) of DSS-treated *GSDMD*$^{fl/fl}$*LysM*-Cre and littermate control *GSDMD*$^{fl/fl}$ mice that were deleted of neutrophils. (**L** and **M**) Flow cytometric analysis of colon-infiltrated immune cells of DSS-treated *GSDMD*$^{fl/fl}$*LysM*-Cre and littermate control *GSDMD*$^{fl/fl}$ mice that were deleted of neutrophils. Data are presented as representative plots (L) and summary graphs of absolute cell numbers (M). Data are pooled from three independent experiments. Error bars show means ± SEM. *$P < 0.05$,, **$P < 0.01$, and ***$P < 0.001$. Two-way ANOVA with Sidak's multiple comparisons test for weight changes and DAI and two-tailed unpaired Student's *t* test for colon length, histology scores, and FACS.

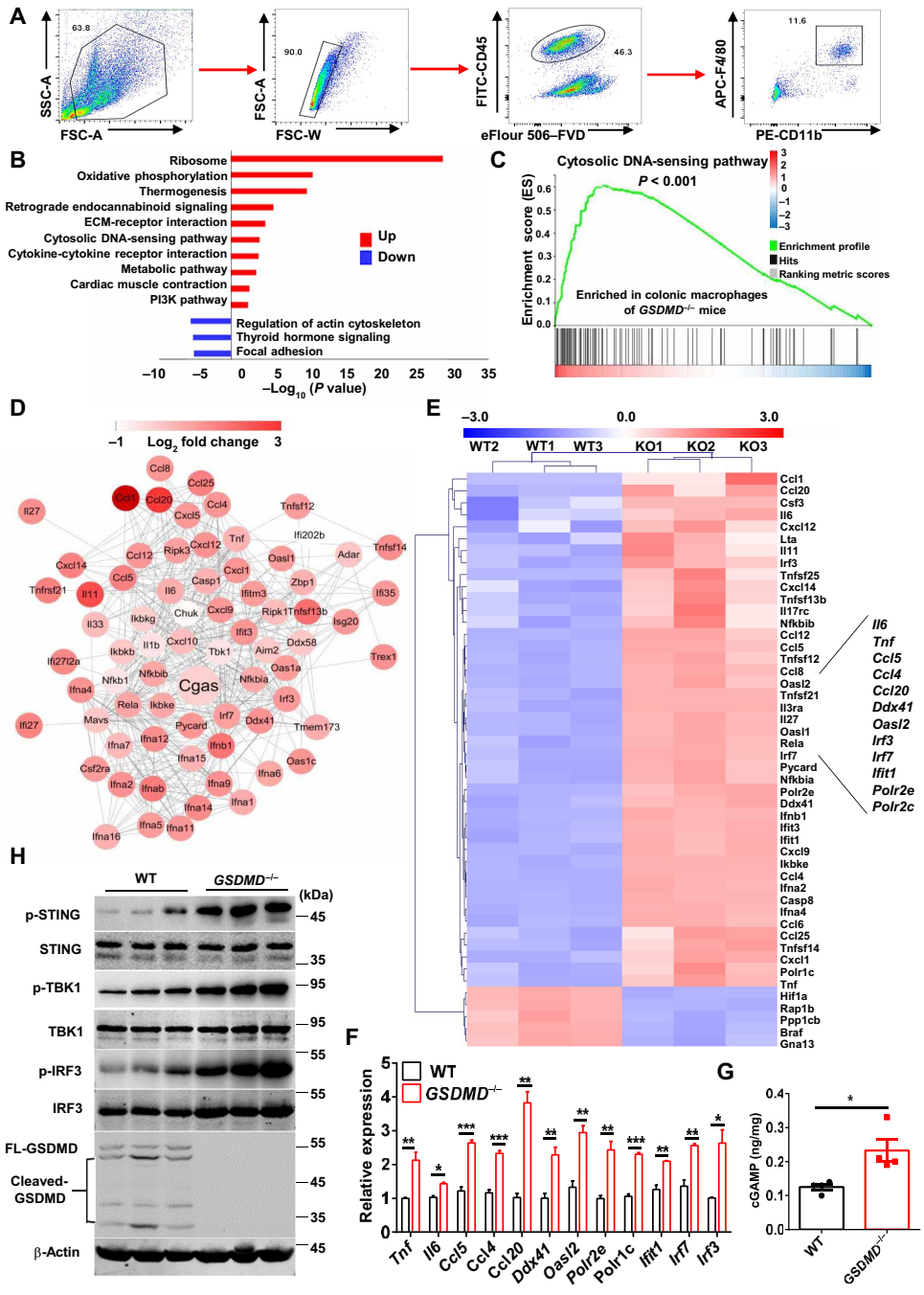

Fig. 4. GSDMD deficiency enhanced cytosolic DNA-sensing pathway in colonic macrophages during colitis. (**A**) FACS gating strategy for sorting colonic macrophages. SSC-A, side scatter area; FSC-A, forward scatter area; FSC-W, forward scatter width. (**B**) KEGG analysis of the most significantly enriched signaling pathways in colonic macrophages sorted from WT and *GSDMD*$^{-/-}$ mice on day 5 after DSS treatment. ECM, extracellular matrix; PI3K, phosphatidylinositol 3-kinase. (**C**) GSEA for the genes associated with "Cytosolic DNA-sensing pathway" in colonic macrophages sorted from mice in (B). Nominal $P < 0.001$. (**D**) Gene Network Analysis of the genes associated with cytosolic DNA-sensing pathway in colonic macrophages sorted from mice in (B). Node colors increasing from white to red indicate expression-level changes in *GSDMD*$^{-/-}$ cells relative with WTs. (**E**) Heatmaps of genes with adjusted $P < 0.05$ and $\log_2$ fold change >1.2 from RNA-seq analysis of colonic macrophages sorted from mice in (B). (**F**) RT-qPCR analysis of the indicated genes in colonic macrophages sorted from mice in (B). Data were normalized to a reference gene, *HPRT*. (**G**) UPLC/MS analysis of cGAMP levels in colonic tissues from WT and *GSDMD*$^{-/-}$ mice ($n = 4$ mice per group) on day 9 after DSS treatment. (**H**) Immunoblot analysis of phosphorylated (p-) STING, STING, phosphorylated (p-) TBK1, TBK1, phosphorylated (p-) IRF3, IRF3, GSDMD, and β-actin (loading control) in colons from DSS-treated WT and *GSDMD*$^{-/-}$ mice on day 9. Data are representative of two independent experiments (H). Error bars show means ± SEM. *$P < 0.05$, **$P < 0.01$, and ***$P < 0.001$. Two-tailed unpaired Student's *t* test.

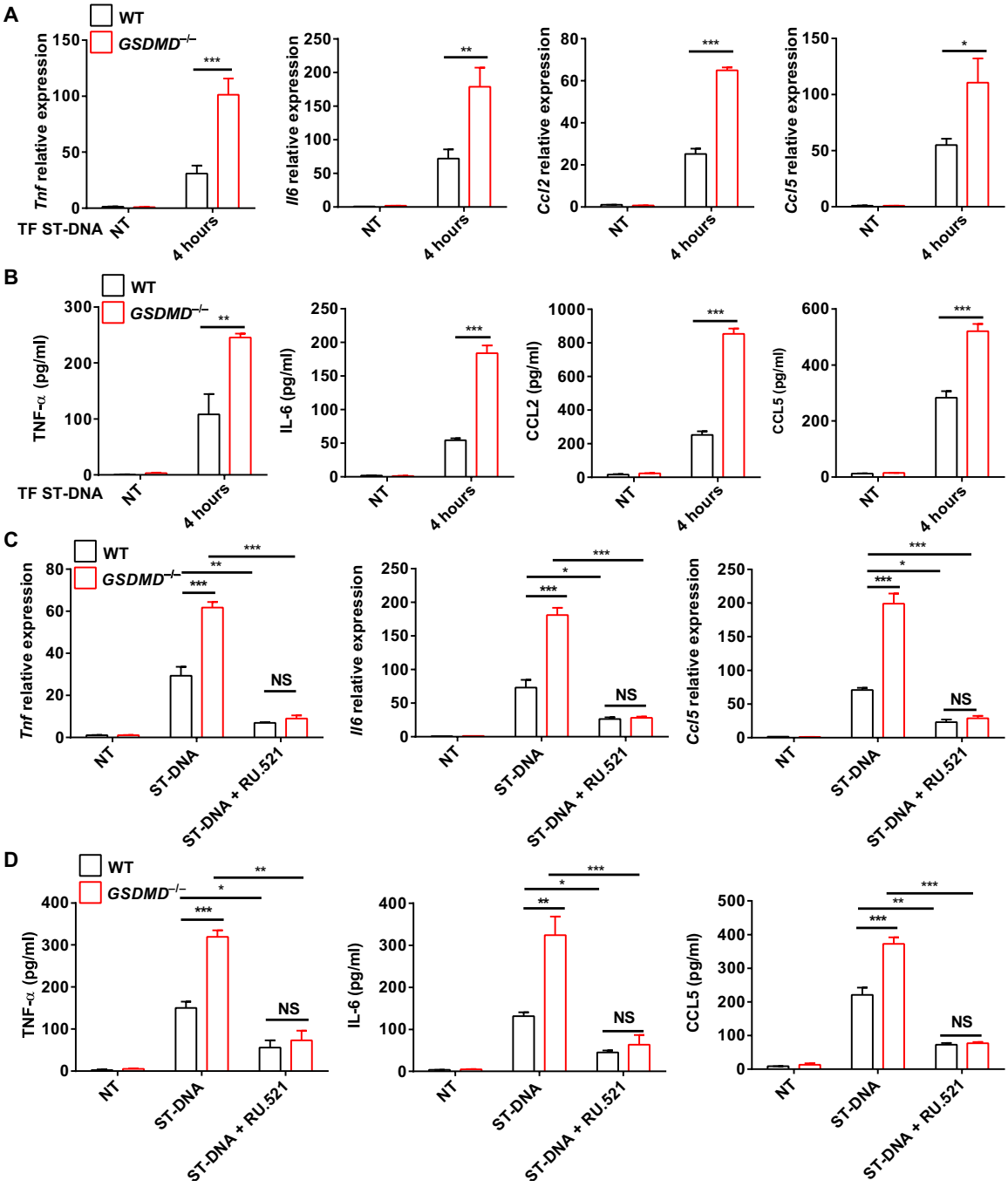

Fig. 5. GSDMD deficiency enhanced cGAS-dependent inflammation in colonic macrophages. (**A** and **B**) $CD45^+CD11b^+F4/80^+$ colonic macrophages were sorted from the LP of WT and *GSDMD*$^{-/-}$ mice and then were transfected with gDNA from *Salmonella Typhimurium* (ST-DNA) for 4 hours. The mRNA expression or protein production of the indicated cytokines and chemokines was analyzed by RT-qPCR (C) or ELISA (D), respectively. (**C** and **D**) $CD45^+CD11b^+F4/80^+$ colonic macrophages from LP of WT mice and *GSDMD*$^{-/-}$ mice were treated with cGAS inhibitor RU.521 (20 μg/ml) and then were transfected with ST-DNA for 4 hours. The mRNA expression or protein production of indicated cytokines and chemokines was analyzed by RT-qPCR (**E**) or ELISA (**F**), respectively. Data are pooled from three independent experiments. Error bars show means ± SEM. **P* < 0.05, ***P* < 0.01, and ****P* < 0.001. Two-way ANOVA with Sidak's multiple comparisons test.

such as caspase-1, ASC, NLRP6, or NLRP12, play protective roles in experimental colitis in a microbiota-dependent manner (*16*, *32*). A previous study demonstrated that NLRP6, ASC, and caspase-1 are required for mucin granule exocytosis by regulating autophagy in goblet cells, which regulates the formation of the inner mucus layer to maintain intestinal barrier integrity (*17*). However, a recent study argued against the concept that Nlrp6 inflammasome is involved in the inner mucus layer formation or function (*18*). In addition, there are some studies concluding that the inflammasome substrate cytokine IL-18 promotes intestinal barrier integrity by enhancing epithelial

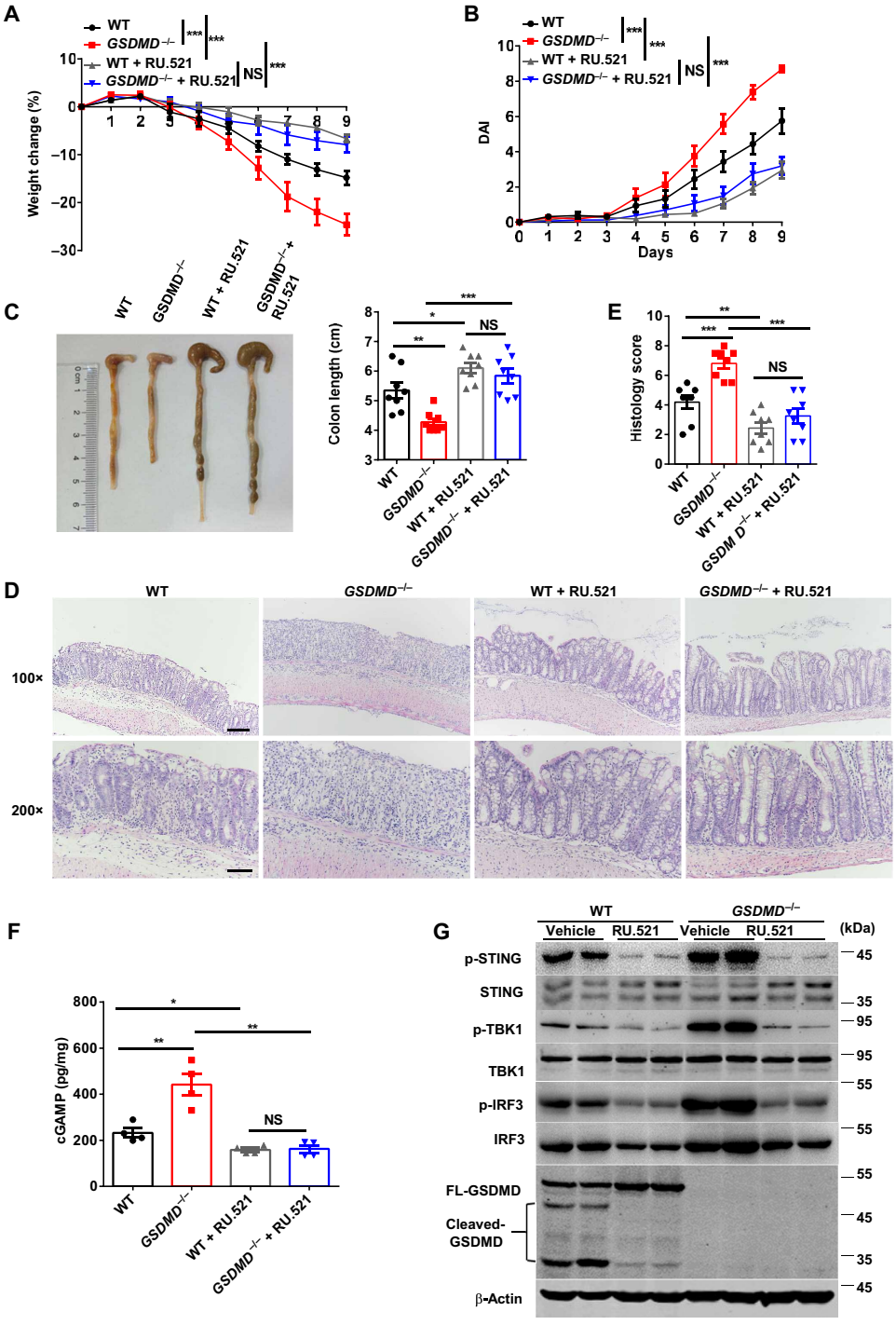

Fig. 6. The administration of cGAS inhibitor restricts colitis in *GSDMD*$^{-/-}$ mice. (**A** to **C**) Age-matched male WT ($n = 8$) and *GSDMD*$^{-/-}$ ($n = 8$) mice were intraperitoneally injected with cGAS inhibitor RU.521 at a dose of 10 mg/kg daily after DSS treatment. Weight changes (A), DAI (B), and colon lengths (C) of DSS-treated WT and *GSDMD*$^{-/-}$ mice that were injected with cGAS inhibitor. (**D** and **E**) Representative H&E staining section of colons (D) and histology score (E) of mice in (A). Scale bars, 100×, 100 μm; 200×, 200 μm. (**F**) ELISA of cGAMP levels in colonic tissue homogenates of mice on day 9 after DSS treatment ($n = 4$ mice per group). (**G**) Immunoblot analysis of phosphorylated STING, STING, phosphorylated TBK1, TBK1, phosphorylated IRF3, IRF3, GSDMD, and β-actin (loading control) in colons from WT and *GSDMD*$^{-/-}$ mice that were administrated with cGAS inhibitor RU.521. Data are pooled from three independent experiments (A to E) or are representative of two independent experiments (G). Error bars show means ± SEM. $^{*}P < 0.05$, $^{**}P < 0.01$, and $^{***}P < 0.001$. Two-way ANOVA with Sidak's multiple comparisons test for weight changes and DAI and two-tailed unpaired Student's *t* test for colon length and histology scores. Photo credit: (C) was taken by C.M. (Department of Immunology, Nanjing Medical University).

proliferation during early colitis (*33*). Moreover, IL-18 is thought to regulate the production of AMPs and shape the homeostasis of microbiome, thereby avoiding the outgrowth of colitogenic microbiota (*14*). Conversely, another recent study claimed a pro-colitogenic role for IL-18 in colitis by inhibiting goblet cell maturation, indicating a dichotomous role of IL-18 in colitis (*15*). Thus, the regulatory roles of inflammasome are quite complicated in the intestinal immune system. The underlying mechanism through which the inflammasome in colitis functions and its overall relevance to IBD remain to be investigated. Consistent with many other inflammasome proteins, we found that GSDMD, as the executioner of inflammasome downstream pyroptosis, highly protected against experimental colitis, as characterized by enhanced weight loss and clinical scores in *GSDMD*$^{-/-}$ mice during colitis. However, unlike ASC and NLRP6, cohousing experiments using littermate controls revealed that GSDMD plays a protective role in colitis in a microbiota-independent manner even though the microbiota including some colitogenic strains appear in *GSDMD*$^{-/-}$ mice and are transmissible to cohoused WT mice. This intriguing result suggests that GSDMD uses different mechanism with other inflammasome proteins to be involved in regulating colitis, thus expanding our insights into the complex regulatory mechanisms of inflammasome components in controlling colitis.

While previous studies have suggested that inflammasomes, mainly in IECs, protected against colitis by maintaining intestinal barrier integrity and regulating gut microbiota (*34*), we used cell-type specific conditional knockout mice to reveal a different functional mechanism of GSDMD, which controls colitis by myeloid cells. The expression of GSDMD was high in epithelial cells, but we have not found a role for GSDMD in this cell type in colitis. In a DSS-induced colitis model, the severe damage to the epithelial monolayer lining the large intestine by DSS leads to the rapid dissemination of intestinal Gram-positive or Gram-negative bacteria into the submucosa, which promptly stimulates immune cells in the LP and leads to an acute inflammatory response (*35*). Thus, we speculate that the role of GSDMD in epithelial cells may be masked by massive epithelial cell damage in the DSS model. However, we do not rule out the possibility that GSDMD in IECs may play some role in defenses against intestinal pathogen infection. It has been reported that GSDMD can mediate IEC pyroptosis to remove pathogen-infected epithelial cells (*24*, *36*). We found that in the absence of neutrophils, GSDMD deficiency in macrophages alone still led to exacerbated colitis, thus further establishing GSDMD as a negative regulator of colitis that functions in macrophages. Next, we performed RNA-seq analysis of colonic macrophages from WT and *GSDMD*$^{-/-}$ mice at the onset stage of colitis and revealed that one of the most prominent up-regulated pathways in *GSDMD*$^{-/-}$ macrophages of colitis was associated with the cGAS DNA-sensing pathway. Significant increases in mRNA levels of *Ifit1*, *Oasl2*, *Irf7*, *Irf3*, *Ddx41*, *Il6*, *Tnf*, *Ccl20*, *Ccl4*, and *Ccl5* that were cGAS signaling inducible were identified in colonic macrophages from *GSDMD*$^{-/-}$ mice. IL-6, TNF-α, Cxcl10, Ccl2, and Ccl5 are known to be important proinflammatory cytokines and chemokines for mucosal inflammation, and an abundance of previously published reports has demonstrated their critical roles in the development of IBD (*37*, *38*). Therefore, GSDMD negatively regulates the expression of cytokines and chemokines involved in the cGAS-dependent inflammation pathway in colonic macrophages, which are probably responsible for its role in controlling colitis. Accordingly, a recent study showed that GSDMD deficiency promotes cGAS-mediated inflammation by reducing intracellular potassium (K^+) efflux through GSDMD-formed pores in response to cytosolic DNA or *F. novicida* bacterial infection (*23*). Notably, earlier work has already revealed that cGAS-STING signaling interacts with host commensal bacteria and facilitates colitis (*31*). Moreover, extracellular bacteria and dying cells have been reported to release cyclic dinucleotides to activate activation of cGAS-STING–mediated inflammation in macrophages (*39*). Thus, GSDMD in colonic macrophages may restrain the development of colitis by promoting K^+ efflux via its formed pores to control cGAS-dependent inflammation, in response to invading intestinal bacteria or damaged intestine epithelium. When we directly assessed the effects of cGAS inhibition on colitis in *GSDMD*$^{-/-}$ mice by intraperitoneal administration with cGAS inhibitor RU.521, we found that RU.521 treatment greatly attenuated the colitis severity in *GSDMD*$^{-/-}$ mice.

Together, our study describes an unexpected physiological role of pyroptosis executioner GSDMD in experimental colitis. We propose a model in which GSDMD in colonic macrophages controls cGAS-mediated inflammation in response to invading intestinal bacteria or damaged intestine epithelium after mucosal barrier damage, thereby protecting against the development of colitis (fig. S7). Thus, the development of diagnostic and therapeutic strategies to specifically target GSDMD-cGAS signaling might be useful for protection against IBD.

MATERIALS AND METHODS

Mice

Male mice with the C57BL/6 background were used in this study. The *GSDMD*$^{-/-}$ mice were provided by F. Shao [National Institute of Biological Sciences (NIBS), China]. The *ASC*$^{-/-}$ mice were a gift from V. Dixit (Genentech). The *GSDMD*$^{fl/fl}$ mice were generated using conditional gene targeting methods by Cyagen Biosciences Inc. (Guangzhou, China) as described previously (*21*). *GSDMD*-floxed mice were crossed with *lysozyme M*-Cre mice (*LysM*-Cre; the Jackson laboratory) to generate myeloid cell–conditional *GSDMD* knockout mice (*GSDMD*$^{fl/fl}$ *LysM*-Cre) or with *Villin*-Cre mice (the Jackson laboratory) to produce IEC-conditional *GSDMD* knockout mice (*GSDMD*$^{fl/fl}$ *Villin*-Cre). *Rosa26-tdTomato* mice were crossed with *Cx3cr1*-Cre mice to mark LP macrophages, and *Rosa26-tdTomato* and *Cx3cr1*-Cre mice were provided by J. Zhou (Institute of Neuroscience, Chinese Academy of Sciences). For cohousing experiments, age-matched male WT and knockout mice from the littermates of heterozygous breedings were cohoused at 1:1 ratio for 6 weeks. All mice were kept in a barrier facility, and all animal experiments were conducted in accordance with the procedure approved by the Ethical Review Committee for Laboratory Animal Welfare of the Nanjing Medical University.

Antibodies and reagents

Antibodies to GSDMD (ab219800 and ab209845) and MUC2 (AB76774) were from Abcam. Anti–α-tubulin (T9026) and anti–β-actin (A1978) were from Sigma-Aldrich. Anti–caspase-11 (NB120-10454) was supplied from Novus Biologicals. Anti-ASC (sc-22514) was from Santa Cruz Biotechnology. Anti-phosphorylated STING (72971s), anti-STING (13647s), anti-phosphorylated IRF3 (4947s), anti-IRF3 (4302s), anti-TBK1 (3013s), and anti-phosphorylated TBK1 (5483s) were from Cell Signaling Technology. DSS (DB001-38) was from TdB Consultancy. PAS staining kit was from Servicebio

(G1008). Alcian blue staining kit was from Solarbio (G1560). Anti–CD45–fluorescein isothiocyanate (FITC) (30-F11,11-0451-82), anti–CD8a–phycoerythrin (PE) (53-6.7,12-0081-83), anti–CD45-AF700 (30-F11,85-11-0112-81), anti–CD11b-FITC (M1/70,85-12-0114-81), anti-F4/80 (BM8,17-4801-82), anti–Ly6c-PE-Cy7 (HK1.4,25-5932-82), anti–Ly6g–eFlour 450 (1A8-LY6G,48-9668-82), and FVD (fixable viability dyes)–eFlour 506 (65-0866) were from eBioscience. Anti–CD4-APC (allophycocyanin)–Cy7 (GK1.5,100414) was from Bio-Legend. Anti–CD11b-PE (M1/70, 557397) was from BD Biosciences.

DSS-induced colitis

For acute experimental colitis induction, WT and *GSDMD*$^{-/-}$ mice were treated with 2.5% DSS in their drinking water for 6 days, followed by normal drinking water until the end of the experiment on day 9. For the neutrophil-deletion experiment, mice were injected intravenously with anti-mouse Ly6g antibody (BE0075-1; Bio X Cell) at the dose of 100 μg per mouse starting at 1 day before DSS challenge and then injected with the antibody another three times at days 2, 5, and 8. During the experiment, body weights, stool, and body posture were monitored daily to assess DAI. The DAI is the combined score of weight loss compared with initial weight, stool consistency, and body posture. The scores were evaluated as follows: weight loss: 0 (no loss), 1 (5 to 10%), 2 (10 to 15%), and 3 (>15%); stool consistency: 0 (normal), 1 (mild loose stool), 2 (loose stool), and 3 (diarrhea and bloody stools); body posture: 0 (smooth fur without a hunchback), 1 (mild fur and hunchback), 2 (moderate fur and hunchback), and 3 (severe fur and heavy hunchback). Mice were euthanized at the indicated time points, and colons were collected immediately for colon length measure, colon explant culture, colonic immune cell analysis, and histology analysis.

Colon explant culture

Colons were excised from mice, washed briefly in phosphate-buffered saline (PBS), and then washed three times with cold PBS containing gentamicin (20 μg/ml), penicillin G (200 μg/ml), and streptomycin (200 μg/ml) to remove residual intestinal bacteria and then was incubated in supplemented culture medium containing penicillin G (200 μg/ml) and streptomycin (200 μg/ml) (*40*). The medium was collected after incubation for 24 hours at 37°C, and the production of proinflammatory cytokines was determined by ELISA.

Real-time quantitative polymerase chain reaction

Total RNA was extracted by using TRIzol reagent (Life) and subjected to complementary DNA synthesis. Reverse transcription products of different samples were amplified by StepOnePlus (Applied Biosystems) using Brilliant SYBR Green QPCR Master Mix (Vazyme) according to the manufacturer's instructions. The following primers were used:

Reg3b	**S**	**As**
	5-AATGGAGGTGGATGGGAATG-3	5-CGGTCTAAGGCAGTAGATGGGT-3
Reg3g	S	As
	5-AACAGAGGTGGATGGGAGTGG-3	5-CACAGTGATTGCCTGAGGAAGA-3
defn5	S	As
	5-GGCTGATCCTATCCACAAAACA-3	5-AGACCCTTCTTGGCCTCCA-3
lysozyme 1	S	As
	5-ACTCTGGGACTCCTCCTGCTT-3	5-CGGTCTCCACGGTTGTAGTTT3-3
Il22	S	As
	5-CCCTTATGGGGACTTTGGC-3	5-GGTGCGGTTGACGATGTATG-3
Muc2	S	As
	5-TTGCTCTGCTGTCTCCGTCA-3	5-ACACTGGTCTTCTCCTCCTTGC-3
Cxcl10	S	As
	5-AAGTGCTGCCGTCATTTTCTG-3	5-TTCCCTATGGCCCTCATTCTC-3
Il-6	S	AS
	5-CTTGGGACTGATGCTGGTGAC-3	5-GCCATTGCACAACTCTTTTCTC-3
Tnf	S	AS
	5-TACTGAACTTCGGGGTGATCG-3	5-TCCTCCACTTGGTGGTTTGC-3
Ccl5	S	AS
	5-GACACCACTCCCTGCTGCTT-3	5-ACACTTGGCGGTTCCTTCG-3
Irf7	S	As
	5-CAGCACAGGGCGTTTTATCTT-3	5-TCTTCCCTATTTTCCGTGGC-3
Ifnb	S	As
	CCCTATGGAGATGA CGGAGA	5-CCCAGTGCTGGAGAAATTGT-3
Irf3	S	As
	5-CTACGGCAGGACGCACAGAT-3	5-TCAGCAGCTAACCGCAACAC-3
Ddx41	S	AS
	5-AGTCCGCCAAGGAAAAGCAA-3	5-CTCAGACATGCTCAGGACATAAC-3
Ifit1	S	AS
	5-TGCTTTGCGAAGGCTCTGA-3	5-AATCTTGGCGATAGGCTACGAC-3
Ccl20	S	AS
	5-TGTACGAGAGGCAACAGTCG-3	5-TCTGCTCTTCCTTGCTTTGG-3
Ccl4	S	AS
	5-GCTCTGTGCAAACCTAACCC-3	5-GAAACAGCAGGAAGTGGGAG-3
Cc12	S	AS
	5-CTGTGCTGACCCCAAGAAGG-3	5-TTGAGGTGGTTGTGGAAAAGG-3
Polr2c	S	AS
	5-CGTGGTTCTCGGAGAGTTTGG-3	5-CCAGCGTGTCTTCATCCATTT-3
Polr2e	S	AS
	5-GGTGGGCATCAAGACCATCAA-3	5-TCAGGGACTAGCTCGTGCTC-3
Cxcl1	S	AS
	5-CACCCAAACCGAAGTCATAGC-3	5-TTGGGGACACCTTTTAGCATCT-3
Asc	S	AS
	5-TCTGGAGTCGTATGGCTTGGA-3	5-AGTGCTTGCCTGTGCTGGTC-3
Gsdmd	S	AS
	5-ATCCTGGCATTCCGAGTGG-3	5-CTCTGGCCCACTGCTTTTCT-3
Hprt	S	AS
	5-GTCCCAGCGTCGTGATTAGC-3	5-TGGCCTCCCATCTCCTTCA-3

Cytokines and cGAMP ELISA

Conditioned supernatants from colon explants or colonic macrophages were collected and measured for levels of IL-6, TNF-α, IL-1β, CCL2, CCL5, CXCL1, and CXCL10 according to the manufacturer's instructions (R&D Systems). The level of IL-18 was assayed by an in-house sandwich ELISA system. For cGAMP assay, colons were

excised and washed thoroughly by flushing with PBS. Colons were weighed and homogenized. The supernatants from colonic homogenates were collected and measured for the levels of cGAMP using ELISA kit (Shanghai Jingkang Bioengineering Co. Ltd., JLC19223).

Ultraperformance liquid chromatography/mass spectrometry analysis

Colonic tissues from WT and *GSDMD*$^{-/-}$ mice were freeze dried for 12 hours and weighed. The freeze-dried tissues were grinded with liquid nitrogen and added with 800 μl of extraction solution [methanol:acetonitrile:water (v/v/v, 4:4:1)]. All the samples were sonicated for 30 min at 4°C and then incubated at −20°C for 1 hour and centrifuged at 12,000 rpm, 4°C for 15 min. Then, 600 μl of supernatant was evaporated and was reconstituted with 100 μl of 80% methanol and then was transferred to an injection vial for liquid chromatography (LC)–mass spectrometry (MS) analysis. For ultraperformance LC (UPLC), the column is an ACQUITY UPLC BEH Ami (100 × 2.1 mm, 1.7 μm), and column temperature is 40°C. Flow rate is 0.35 ml/min. Mobile phase: A, water; B, acetonitrile. Injection volume is 6 μl. MS parameters were as follows: curtain gas, 35 arb (arbitrary units) gas flow rate; collision gas, 7 arb; IonSpray voltage, −4500 V; IonSource temperature, 500°C; IonSource gas1, 50 arb; and IonSource gas2, 50 arb. MRM acquisition parameters: According to the chromatographic and mass spectrometric conditions described above, the prepared standard cGAMP solution (Sigma-Aldrich) was added to the sample vial to quantify and identify the cGAMP peaks at R_t = 2.60 min. Concentration of cGAMP was determined using the following formula: $y = 126.3x + 6.1214$ ($r^2 = 0.9996$) (y, peak area; x, analyte concentration in ng/ml). All values multiplied volume and were converted to that relative to weight by dividing tissue weights.

Histological analysis

For histology, the colons were washed, fixed in 4% buffered formaldehyde, and embedded in paraffin. Tissue sections were stained with H&E. Histology was scored in a blinded fashion as a combination of inflammatory cell infiltrate (score, 0 to 4) and intestinal architecture damage (scores 0 to 4). The presence of occasional inflammatory cells in the LP was scored as 0; increased numbers of inflammatory cells in the LP was scored as 1; inflammatory cells extending into the mucosa and submucosa were scored as 2; inflammatory cells extending into the mucosa, submucosa, and, sometimes, transmural infiltration were scored as 3; and severe transmural extension of the infiltrate was scored as 4. For intestinal architecture damage, no mucosal damage was scored as 0; focal erosions were scored as 1; slight crypt loss and focal ulcerations were scored as 2; extended ulcerations and moderate crypt loss were scored as 3; and extensive crypt loss, mucosal damage, and extension into deeper structures of the bowel wall were scored as 4. The combined histological score ranged from 0 (no changes) to 8 (extensive infiltration and tissue damage). Tissues were stained with PAS for showing goblet cells. Images were acquired with a Nikon 50i inverted microscope.

Immunofluorescence staining

Tissue sections were incubated at 4°C overnight with primary antibody to MUC2, GSDMD, and E-cadherin. Slides were then incubated with indicated secondary antibodies. The nuclei were counterstained with 4′,6-diamidino-2-phenylindole (DAPI) (Sigma-Aldrich). Slides were dried and mounted using ProLong Antifade mounting medium (Beyotime Biotechnology). Slides were visualized using a Nikon 50i fluorescence microscope or a Zeiss LSM 700 META laser scanning confocal microscope.

Immunoblotting

Tissue homogenates were lysed in lysis buffer solution [150 mM NaCl, 10 mM tris (pH 7.4), 5 mM EDTA, 1 mM EGTA, and 0.1% NP-40] supplemented with a protease inhibitor cocktail tablet (Sigma-Aldrich). Samples were clarified, denatured with SDS buffer, and boiled for 10 min. Proteins were separated by SDS–polyacrylamide gel electrophoresis and transferred onto nitrocellulose membranes. The membranes were immunoblotted with primary antibodies and proteins detected with appropriate secondary anti-rabbit antibody conjugated to fluorescence. Immunoreactivity was visualized by the Odyssey Imaging System (LI-COR Biosciences).

Isolation of colonic epithelial and immune cells and FACS analysis and sorting

Colons were excised and washed thoroughly by flushing with PBS for several times. They were opened longitudinally and transferred into Gentle Cell Dissociation Reagent (STEMCELL) and shaken for 20 min at 37°C. The colons were then washed three times with PBS containing 2 mM EDTA. All supernatants were collected and passed through a 100-μm cell strainer to get single-cell suspensions. The single-cell suspensions were collected and stained with anti-CD45 and anti-CD326. IECs (CD326$^+$CD45$^-$) were sorted on a BD FACSAria. The remaining colons were collected to digest for 45 min at 37°C using Dulbecco's modified eagle medium (DMEM) containing 2% fetal bovine serum, collagenase IV (2.5 mg/ml; Sigma-Aldrich), and deoxyribonuclease I (10 U/ml; Roche). Single-cell suspensions were obtained by grinding through a 70-μm cell strainer. Subsequently, homogeneous cell suspensions were centrifuged over the Percoll density (GE Healthcare), and LP immune cells were separated by collecting the interface fractions between 40 and 80% Percoll. After intensive washing, single-cell suspensions were stained with FVD eFlour 506, anti-CD45, anti-CD11b, anti-F4/80, anti-CD4, anti-CD8, anti-Ly6c, and anti-Ly6g for FACS analysis. All flow cytometry was performed on an Attune NxT Flow Cytometer (Thermo Fisher Scientific), and data were analyzed by FlowJo 10 software. For colonic myeloid cell and macrophage sorting, single-cell suspensions were stained with FVD eFlour 506, anti-CD45, anti-CD11b, and anti-F4/80. Myeloid cells (CD326$^-$CD45$^+$CD11b$^+$) and macrophages (CD45$^+$CD11b$^+$F4/80$^+$) were sorted on a BD FACSAria.

Colonic macrophage preparation and stimulation

For isolation of colonic macrophages, colonic single-cell suspensions were stained with FVD eFlour 506, anti-CD45, anti-CD11b, and anti-F4/80 and sorted on a BD FACSAria. Following cell sorting by FACS, the purified macrophages (CD45$^+$CD11b$^+$F4/80$^+$) were cultured for 24 hours in DMEM (Gibco) supplemented with penicillin (100 U/ml), streptomycin (100 μg/ml), and 10% fetal bovine serum (Sigma-Aldrich). The cells were transfected with Lipofectamine 2000 (2 μl/ml)–complexed poly(dA:dT) (1 μg per 10^6 cells) or gDNA derived from *Salmonella* (ST-DNA) (1 μg per 10^6 cells) for 4 hours. For cGAS inhibition experiment, the purified macrophages were primed with RU.521 (20 μg/ml; cGAS inhibitor) for 3 hours before ST-DNA transfection. The conditioned media were collected and measured for cytokine production by ELISA, and the cells were collected for cytokine gene expression by RT-qPCR.

cGAS inhibitor treatment in DSS-induced colitis mice

The cGAS inhibitor RU.521 (AOBIOUS INC.) was dissolved in 10% dimethyl sulfoxide and then was diluted with Corn Oil. The inhibitor was intraperitoneally injected into WT and *GSDMD*$^{-/-}$ mice at a dose of 10 mg/kg daily starting 1 day before DSS challenge.

16*S* ribosomal RNA gene sequencing

Microbial DNA was extracted from fecal samples of the indicated mice by using the TIANamp Stool DNA Kit (TIANGEN) according to the manufacturer's protocols. DNA concentration was assessed by a One Drop, and quality was determined by agarose gel electrophoresis. The V3-V4 regions of the bacteria 16*S* ribosomal RNA gene were amplified by PCR using the flowing primers: 338F 5′-barcode-ACTCCTACGGGAGGCAGCA-3′ and 806R 5′-GGACTACHVG-GGTWTCTAAT-3′ (barcode is an eight-base pair sequence unique to each sample). The PCR products were then extracted from 2% agarose gels and further purified by using the AxyPrep DNA Gel Extraction Kit (Axygen Biosciences) and quantified by QuantiFluor-ST (Promega). The purified DNA amplicons were then added with Illumina adapters by ligation (TruSeq DNA LT Sample Prep Kit), and the adapter-ligated DNA fragments were further pooled in equimolar and paired-end sequenced (2 × 300) on an Illumina MiSeq platform for sequencing according to the standard protocols by Majorbio Bio-Pharm Technology Co. Ltd. (Shanghai, China). Raw fastq files were quality filtered by Trimmomatic and merged by FLASH (Fast Length Adjustment of SHort reads) with the following criteria: (i) The reads were truncated at any site receiving an average quality score <20 over a 50–base pair (bp) sliding window. (ii) Sequences whose overlap being longer than 10 bp were merged according to their overlap with mismatch no more than 2 bp. (iii) Sequences of each sample were separated according to barcodes (exactly matching) and primers (allowing two nucleotide mismatching), and reads containing ambiguous bases were removed. Operational taxonomic units (OTUs) were clustered with 97% similarity cutoff using UPARSE (version 7.1; http://drive5.com/uparse/) with a "greedy" algorithm that performs chimera filtering and OTU clustering simultaneously. The taxonomy of each 16*S* rRNA gene sequence was analyzed by RDP Classifier algorithm (http://rdp.cme.msu.edu/) against the Silva (SSU123) 16*S* rRNA database using a confidence threshold of 70%. The raw reads were deposited into the National Center for Biotechnology Information (NCBI) Sequence Read Archive (SRA) database (SRA accession: PRJNA574780).

RNA-seq analysis

For RNA-seq, CD45^{+}CD11b^{+}F4/80^{+} macrophages were isolated from colons of WT and *GSDMD*$^{-/-}$ mice on day 5 after DSS treatment by sorting on a BD FACSAria. RNA isolation, library construction, and sequencing were performed on a BGISEQ-500 [Beijing Genomic Institution (BGI)]. Clean reads were mapped to the mouse genome (GRCm38.p5) by HISAT2. For gene expression analysis, the matched reads were calculated and then normalized to fragments per kilobase million. Fold changes were calculated for all possible comparisons, and a 1.2-fold cutoff was used to select genes with expression changes. KEGG pathway analysis was performed using the R package, using significantly differentially expressed genes ($P < 0.05$) as target genes. GSEA and Gene Network Analysis were performed to analyze the genes associated with "cytosolic DNA-sensing pathway." The data mining and figure presentation process, including KEGG, GSEA, Gene Network Analysis, the heatmap, and clustering, are all done by the BGI in-house customized data mining system called Dr.Tom (http://report.bgi.com). Raw data files and processed files have been uploaded to the Gene Expression Omnibus public database (GSE137827).

Statistical analyses

The data were analyzed by GraphPad Prism 7.0 software and are presented as the means ± SEM. The statistics were analyzed by using two-tailed unpaired *t* test for two groups or two-way analysis of variance (ANOVA) for multiple groups. *P* values were provided as $*P < 0.05$, $**P < 0.01$, and $***P < 0.001$.

SUPPLEMENTARY MATERIALS

Supplementary material for this article is available at http://advances.sciencemag.org/cgi/content/full/6/21/eaaz6717/DC1

View/request a protocol for this paper from *Bio-protocol*.

REFERENCES AND NOTES

1. M. A. McGuckin, R. Eri, L. A. Simms, T. H. Florin, G. Radford-Smith, Intestinal barrier dysfunction in inflammatory bowel diseases. *Inflamm. Bowel Dis.* **15**, 100–113 (2008).
2. C. N. Bernstein, M. Fried, J. Krabshuis, H. Cohen, R. Eliakim, S. Fedail, R. Gearry, K. Goh, S. Hamid, A. G. Khan, A. W. LeMair, Malfertheiner, Q. Ouyang, J. F. Rey, A. Sood, F. Steinwurz, O. O. Thomsen, A. Thomson, G. Watermeyer, World gastroenterology organization practice guidelines for the diagnosis and management of IBD in 2010. *Inflamm. Bowel Dis.* **16**, 112–124 (2010).
3. Y. Belkaid, T. W. Hand, Role of the microbiota in immunity and inflammation. *Cell* **157**, 121–141 (2014).
4. A. J. Macpherson, N. L. Harris, Interactions between commensal intestinal bacteria and the immune system. *Nat. Rev. Immunol.* **4**, 478–485 (2004).
5. T. T. MacDonald, G. Monteleone, Immunity, inflammation, and allergy in the gut. *Science* **307**, 1920–1925 (2005).
6. L. V. Hooper, D. R. Littman, A. J. Macpherson, Interactions between the microbiota and the immune system. *Science* **336**, 1268–1273 (2012).
7. J. Pott, M. Hornef, Innate immune signalling at the intestinal epithelium in homeostasis and disease. *EMBO Rep.* **13**, 684–698 (2012).
8. V. A. K. Rathinam, S. K. Vanaja, K. A. Fitzgerald, Regulation of inflammasome signaling. *Nat. Immunol.* **13**, 333–342 (2012).
9. T. Bergsbaken, S. L. Fink, B. T. Cookson, Pyroptosis: Host cell death and inflammation. *Nat. Rev. Microbiol.* **7**, 99–109 (2009).
10. M. Ligumsky, P. Simon, F. Karmeli, D. Rachmilewitz, Role of interleukin 1 in inflammatory bowel disease—Enhanced production during active disease. *Gut* **31**, 686–689 (1990).
11. M. A. Williams, A. O'Callaghan, S. Corr, IL-33 and IL-18 in inflammatory bowel disease etiology and microbial interactions. *Front. Immunol.* **10**, 1091 (2019).
12. M. Coccia, O. J. Harrison, C. Schiering, M. J. Asquith, B. Becher, F. Powrie, K. J. Maloy, IL-1β mediates chronic intestinal inflammation by promoting the accumulation of IL-17A secreting innate lymphoid cells and CD4^{+} Th17 cells. *J. Exp. Med.* **209**, 1595–1609 (2012).
13. S.-U. Seo, N. Kamada, R. Muñoz-Planillo, Y. G. Kim, D. Kim, Y. Koizumi, M. Hasegawa, S. D. Himpsl, H. P. Browne, T. D. Lawley, H. L. Mobley, N. Inohara, G. Nuñez, Distinct commensals induce interleukin-1β via NLRP3 inflammasome in inflammatory monocytes to promote intestinal inflammation in response to injury. *Immunity* **42**, 744–755 (2015).
14. M. Levy, C. A. Thaiss, D. Zeevi, L. Dohnalová, G. Zilberman-Schapira, J. A. Mahdi, E. David, A. Savidor, T. Korem, Y. Herzig, M. Pevsner-Fischer, H. Shapiro, A. Christ, A. Harmelin, Z. Halpern, E. Latz, R. A. Flavell, I. Amit, E. Segal, E. Elinav, Microbiota-modulated metabolites shape the intestinal microenvironment by regulating NLRP6 inflammasome signaling. *Cell* **163**, 1428–1443 (2015).
15. R. Nowarski, R. Jackson, N. Gagliani, M. R. de Zoete, N. W. Palm, W. Bailis, J. S. Low, C. C. Harman, M. Graham, E. Elinav, R. A. Flavell, Epithelial IL-18 equilibrium controls barrier function in colitis. *Cell* **163**, 1444–1456 (2015).
16. E. Elinav, T. Strowig, A. L. Kau, J. Henao-Mejia, C. A. Thaiss, C. J. Booth, D. R. Peaper, J. Bertin, S. C. Eisenbarth, J. I. Gordon, R. A. Flavell, NLRP6 inflammasome regulates colonic microbial ecology and risk for colitis. *Cell* **145**, 745–757 (2011).
17. M. Wlodarska, C. A. Thaiss, R. Nowarski, J. Henao-Mejia, J.-P. Zhang, E. M. Brown, G. Frankel, M. Levy, M. N. Katz, W. M. Philbrick, E. Elinav, B. B. Finlay, R. A. Flavell, NLRP6 inflammasome orchestrates the colonic host-microbial interface by regulating goblet cell mucus secretion. *Cell* **156**, 1045–1059 (2014).

18. J. K. Volk, E. E. Nyström, S. van der Post, B. M. Abad, B. O. Schroeder, Å. Johansson, F. Svensson, S. Jäverfelt, M. E. Johansson, G. C. Hansson, G. M. H. Birchenough, The Nlrp6 inflammasome is not required for baseline colonic inner mucus layer formation or function. *J. Exp. Med.* **216**, 2602–2618 (2019).
19. J. Shi, Y. Zhao, K. Wang, X. Shi, Y. Wang, H. Huang, Y. Zhuang, T. Cai, F. Wang, F. Shao, Cleavage of GSDMD by inflammatory caspases determines pyroptotic cell death. *Nature* **526**, 660 (2015).
20. X. Liu, Z. Zhang, J. Ruan, Y. Pan, V. G. Magupalli, H. Wu, J. Lieberman, Inflammasome-activated gasdermin D causes pyroptosis by forming membrane pores. *Nature* **535**, 153–158 (2016).
21. S. Li, Y. Wu, D. Yang, C. Wu, C. Ma, X. Liu, P. N. Moynagh, B. Wang, G. Hu, S. Yang, Gasdermin D in peripheral myeloid cells drives neuroinflammation in experimental autoimmune encephalomyelitis. *J. Exp. Med.* **216**, 2562–2581 (2019).
22. N. Kayagaki, I. B. Stowe, B. L. Lee, K. O'Rourke, K. Anderson, S. Warming, T. Cuellar, B. Haley, M. Roose-Girma, Q. T. Phung, P. S. Liu, J. R. Lill, H. Li, J. Wu, S. Kummerfeld, J. Zhang, W. P. Lee, S. J. Snipas, G. S. Salvesen, L. X. Morris, L. Fitzgerald, Y. Zhang, E. M. Bertram, C. C. Goodnow, V. M. Dixit, Caspase-11 cleaves gasdermin D for non-canonical inflammasome signalling. *Nature* **526**, 666–671 (2015).
23. I. Banerjee, B. Behl, M. Mendonca, G. Shrivastava, A. J. Russo, A. Menoret, A. Ghosh, A. T. Vella, S. K. Vanaja, S. N. Sarkar, K. A. Fitzgerald, V. A. K. Rathinam, Gasdermin D restrains type I interferon response to cytosolic DNA by disrupting ionic homeostasis. *Immunity* **49**, 413–426. e5 (2018).
24. S. Zhu, S. Ding, P. Wang, Z. Wei, W. Pan, N. W. Palm, Y. Yang, H. Yu, H.-B. Li, G. Wang, X. Lei, M. R. de Zoete, J. Zhao, Y. Zheng, H. Chen, Y. Zhao, K. A. Jurado, N. Feng, L. Shan, Y. Kluger, J. Lu, C. Abraham, E. Fikrig, H. B. Greenberg, R. A. Flavell, Nlrp9b inflammasome restricts rotavirus infection in intestinal epithelial cells. *Nature* **546**, 667–670 (2017).
25. J. R. Turner, Intestinal mucosal barrier function in health and disease. *Nat. Rev. Immunol.* **9**, 799–809 (2009).
26. M. Saleh, G. Trinchieri, Innate immune mechanisms of colitis and colitis-associated colorectal cancer. *Nat. Rev. Immunol.* **11**, 9–20 (2011).
27. P. Orning, E. Lien, K. A. Fitzgerald, Gasdermins and their role in immunity and inflammation. *J. Exp. Med.* **216**, 2453–2465 (2019).
28. C. L. Abram, G. L. Roberge, Y. Hu, C. A. Lowell, Comparative analysis of the efficiency and specificity of myeloid-Cre deleting strains using ROSA-EYFP reporter mice. *J. Immunol. Methods* **408**, 89–100 (2014).
29. X. Cai, Y.-H. Chiu, Z. J. Chen, The cGAS-cGAMP-STING pathway of cytosolic DNA sensing and signaling. *Mol. Cell* **54**, 289–296 (2014).
30. J. Vincent, C. Adura, P. Gao, A. Luz, L. Lama, Y. Asano, R. Okamoto, T. Imaeda, J. Aida, K. Rothamel, T. Gogakos, J. Steinberg, S. Reasoner, K. Aso, T. Tuschl, D. J. Patel, J. F. Glickman, M. Ascano, Small molecule inhibition of cGAS reduces interferon expression in primary macrophages from autoimmune mice. *Nat. Commun.* **8**, 750 (2017).
31. J. Ahn, S. Son, S. C. Oliveira, G. N. Barber, STING-dependent signaling underlies IL-10 controlled inflammatory colitis. *Cell Rep.* **21**, 3873–3884 (2017).
32. G. Y. Chen, Role of Nlrp6 and Nlrp12 in the maintenance of intestinal homeostasis. *Eur. J. Immunol.* **44**, 321–327 (2014).
33. K. Oficjalska, M. Raverdeau, G. Aviello, S. C. Wade, A. Hickey, K. M. Sheehan, S. C. Corr, E. W. Kay, L. A. O'Neill, K. H. Mills, Protective role for caspase-11 during acute experimental murine colitis. *J. Immunol.* **194**, 1252–1260 (2015).
34. A. C. Lei-Leston, A. G. Murphy, K. J. Maloy, Epithelial cell inflammasomes in intestinal immunity and inflammation. *Front. Immunol.* **8**, 1168 (2017).
35. B. Chassaing, J. D. Aitken, M. Malleshappa, M. Vijay-Kumar, Dextran sulfate sodium (DSS)-induced colitis in mice. *Curr. Protoc. Immunol.* **104**, 15 25 11–15 25 14 (2014).
36. I. Rauch, K. A. Deets, D. X. Ji, J. von Moltke, J. L. Tenthorey, A. Y. Lee, N. H. Philip, J. S. Ayres, I. E. Brodsky, K. Gronert, R. E. Vance, NAIP-NLRC4 inflammasomes coordinate intestinal epithelial cell expulsion with eicosanoid and IL-18 release via activation of caspase-1 and -8. *Immunity* **46**, 649–659 (2017).
37. H. C. Reinecker, M. Steffen, T. Witthoeft, I. Pflueger, S. Schreiber, R. MacDermott, A. Raedler, Enhand secretion of tumour necrosis factor-alpha, IL-6, and IL-1β by isolated lamina ropria monouclear cells from patients with ulcretive cilitis and Crohn's disease. *Clin. Exp. Immunol.* **94**, 174–181 (1993).
38. D. Wang, R. N. DuBois, A. Richmond, The role of chemokines in intestinal inflammation and cancer. *Curr. Opin. Pharmacol.* **9**, 688–696 (2009).
39. H. Liu, P. Moura-Alves, G. Pei, H. J. Mollenkopf, R. Hurwitz, X. Wu, F. Wang, S. Liu, M. Ma, Y. Fei, C. Zhu, A. B. Koehler, D. Oberbeck-Mueller, K. Hahnke, M. Klemm, U. Guhlich-Bornhof, B. Ge, A. Tuukkanen, M. Kolbe, A. Dorhoi, S. H. Kaufmann, cGAS facilitates sensing of extracellular cyclic dinucleotides to activate innate immunity. *EMBO Rep.* **20**, e46293 (2019).
40. S. Wirtz, C. Neufert, B. Weigmann, M. F. Neurath, Chemically induced mouse models of intestinal inflammation. *Nat. Protoc.* **2**, 541–546 (2007).

Acknowledgments: We thank F. Shao (NIBS, Beijing, China) for *GSDMD*$^{-/-}$ mice.
Funding: This work was supported by the National Natural Science Foundation of China (81570499/91742116/81771773 to S.Y., 81802393 to B.W., and 81901227 to C.M.), the Thousand Young Talents Plan of China (S.Y.), the Start Fund for Specially-Appointed Professor of Jiangsu Province (S.Y.), the Plan of Jiangsu Innovative and Entrepreneurial team (303073227 to S.Y.), the Major Project of the Nanjing Medical University Science and Technology Development Fund (NMUD2018003 to S.Y.), the cultivation project of "high level young scientific and technological talents" of Nanjing Medical University (NMUR2019003 to S.Y.), the Natural Science Youth Foundation of Jiangsu Province (BK20180679 C.M.), and the Roche Postdoctoral Fellowship (RPF) program (C.M.). **Author contributions:** C.M., D.Y., C.W., Y.W., S.L., and X.L. designed and performed the experiments, analyzed the data, and prepared the figures. B.W. provided the key technique mentoring and research reagents. B.W., K.L., and L.D. contributed to the experimental design and edited the manuscript. K.L., L.D., and S.Y. supervised the project. C.M. and S.Y. wrote the manuscript. **Competing interests:** The authors declare that they have no competing interests. **Data and materials availability:** Sequencing data are deposited into the GEO (accession nos. PRJNA574780 and GSE137827). All data needed to evaluate the conclusions in the paper are present in the paper and/or the Supplementary Materials. Additional data related to this paper may be requested from the authors.

Submitted 29 September 2019
Accepted 9 March 2020
Published 20 May 2020
10.1126/sciadv.aaz6717

Citation: C. Ma, D. Yang, B. Wang, C. Wu, Y. Wu, S. Li, X. Liu, K. Lassen, L. Dai, S. Yang, Gasdermin D in macrophages restrains colitis by controlling cGAS-mediated inflammation. *Sci. Adv.* **6**, eaaz6717 (2020).

Science Advances

Gasdermin D in macrophages restrains colitis by controlling cGAS-mediated inflammation

Chunmei Ma, Dongxue Yang, Bingwei Wang, Chunyan Wu, Yuqing Wu, Sheng Li, Xue Liu, Kara Lassen, Lue Dai and Shuo Yang

Sci Adv **6** (21), eaaz6717.
DOI: 10.1126/sciadv.aaz6717

Science Advances (ISSN 2375-2548) is published by the American Association for the Advancement of Science, 1200 New York Avenue NW, Washington, DC 20005. The title *Science Advances* is a registered trademark of AAAS.